

# Near-field scanning optical microscopy of ZnO nanopatterns fabricated by micromolding in capillaries

S. K. Donthu, Z. Pan, G. S. Shekhawat, and V. P. Dravid<sup>a)</sup>

*Department of Materials Science and Engineering, Northwestern University, Evanston, Illinois 60208*

B. Balakrishnan and S. Tripathy

*Institute of Materials Research and Engineering, 3 Research Link, Singapore 117602, Singapore*

(Received 4 February 2005; accepted 19 May 2005; published online 19 July 2005)

We report near-field scanning optical microscopy (NSOM) studies of 300-nm-wide ZnO nanopatterns fabricated by micromolding in capillary technique using a sol-gel route. Atomic force microscopy and scanning electron microscopy show that the patterns are continuous with uniform linewidths. Simultaneous topography and optical signal collected in NSOM scans exhibit nanoscale photoluminescence intensity distribution in the ZnO nanopatterns. The nanoscale spectral mapping shows very broad defect-induced green-yellow-red luminescence bands, at room temperature, when excited with a 514.5-nm Ar-ion laser. Our analyses demonstrate that spatially resolved ZnO luminescence features with an optical resolution of  $\leq 300$  nm can be obtained with NSOM while operating in collection mode, and underscore the need to couple nanoscale physical characterization with functional properties at the same scale. © 2005 American Institute of Physics.

[DOI: 10.1063/1.1949712]

## INTRODUCTION

ZnO is an important wide-band-gap semiconductor with numerous potential applications such as sensors, varistors,<sup>1</sup> surface acoustic wave devices,<sup>2</sup> and short-wavelength light-emitting devices.<sup>3–5</sup> Photoluminescence (PL) is an important physical property that reflects the optical quality of ZnO. Like many other physical properties, PL in ZnO is critically influenced by microstructure which in turn depends on fabrication routes and processing conditions. For example, PL properties of several types of ZnO nanostructures, such as nanowires, nanotubes, and tetrapods,<sup>6–8</sup> have been reported and are shown to be different from ZnO single crystal.<sup>9</sup> In addition PL properties of ZnO even in thin films made from different technique are known to be different. The most widely accepted premise for this strong influence of fabrication routes on optical properties of ZnO is the dependence of concentration of structural defects on deposition technique.

Several types of defects, such as oxygen vacancies ( $V_O$ ), zinc interstitials ( $Zn_i$ ), zinc vacancies ( $V_{Zn}$ ), and antisite defects ( $O_{Zn}$ ), are known to dramatically influence the optical properties of ZnO. On the other hand, in order to build nanoscale functional devices it is essential to have control over site- and shape-specific positioning of nanostructures. This continues to prove challenging, especially for large-scale aerial coverage. In this context, localized but large-scale nanopatterning is an attractive route to fabricate functional nanostructures. The ability to pattern technologically significant oxides, such as ZnO at submicron scale over large areas, will have a major impact on the development of miniaturized and/or integrated multifunctional devices. Because the optical properties of the nanopatterns strongly depend on

the patterning technique, there is a continuing need for their characterization with a suitable nanoscale measurement technique.

Micromolding in capillaries (MIMICs) is a versatile patterning technique with a flexibility to pattern variety of materials and with the ability to rapidly pattern areas in excess of several centimeters.<sup>10–13</sup> Although MIMIC technique has been used to pattern several materials with feature sizes in micron range,<sup>10</sup> reports on fabrication of pattern features in nanometer range using this technique are particularly rare. Moreover, most of these reports show only the basic structural characterization of pattern using x-ray diffraction (XRD), atomic force microscopy (AFM), and electron microscopy. Clearly, measurement of local optical properties of these patterns is critical to validate their functionality and to benchmark them for practical applications.

Near-field scanning optical microscopy (NSOM) is emerging as a powerful analytical tool, capable of subwavelength spatial resolution that is ideally suited to investigate optical properties of nanostructures.<sup>14–16</sup> Versatility of the NSOM is highlighted by reports investigating varied phenomenon such as photonic block copolymer morphology,<sup>17</sup> fluorescence imaging of biological samples,<sup>15</sup> imaging of second-harmonic generation in ZnO nanowires,<sup>18</sup> observation of local ferroelectric phase transitions,<sup>19</sup> and among many others. With significant technological advances in NSOM tip fabrication and with major advances in instrumentation, NSOM will continue to serve as a valuable tool to probe optical properties of nanostructures. In addition, operating NSOM in collection mode, where emission signal from sample is collected in near field using NSOM tip, is valuable for optical property measurements of nanopatterns which may not show strong luminescence compared to monolithic nanostructures such as nanorods. In this article, we report the

<sup>a)</sup>Electronic mail: v-dravid@northwestern.edu

spatially varying PL properties and optical quality of ZnO nanopatterns using NSOM operating in collection mode.

## EXPERIMENT

Zinc oxide solution was prepared by stirring a mixture of zinc acetate dihydrate (1.54 g), 2-methoxy ethanol (19.6 ml), and ethanolamine (0.4 ml) at 60 °C for 2 h. This gives a 0.35-M ZnO solution. This solution formulation is transparent and remains stable for more than 6 months. A polydimethylsiloxane (PDMS) elastomer mold was used for MIMIC patterning, which was made from a submillimeter thin film obtained by spin-coating elastomer on a gold grating (Edmund Optics, 1200 grooves/mm and a glazing angle of 36° 52'). After curing at 70 °C for about 10 h, the PDMS film was carefully peeled off from the Au grating (master mold) and placed on top of SiO<sub>x</sub>/Si substrate that was previously cleaned thoroughly in acetone, piranha (3:1 volume ratio of H<sub>2</sub>SO<sub>4</sub>:H<sub>2</sub>O<sub>2</sub>) solution at 70 °C, and finally with de-ionized (DI) water. A droplet of ZnO solution placed at the entrance of capillaries quickly fills the channels. The whole substrate was then moved into a vacuum chamber for 2 h to enhance degassing from PDMS stamp and liquid infusion into the channels. The substrate was then slightly heated at temperatures between 60 and 70 °C for 2 h to evaporate the solvent. The mold was subsequently peeled off and the patterns were annealed at 550 °C for 1 h in air.

NSOM measurements (The MultiView 1000™, Nanonics Imaging Ltd.) were done in both illumination and collection modes using Cr/Al-coated cantilevered optical fiber probes with 200- and 300-nm aperture diameters. In both modes, Ar-ion laser ( $\lambda=514.5$  nm, 10 mW output power) coupled to the optical fiber was used to excite the defect induced luminescent states in ZnO nanopatterns. Images in “constant-amplitude” mode were obtained with the normal force feedback loop to maintain constant tip distance from the surface, while the “constant-height” images were obtained by scanning with feedback mode turned off. NSOM-PL intensity mapping was carried out using an avalanche photodiode (APD) with single-photon counting electronics. Specific optical filters were used for efficient detection of reflected or luminescent light from ZnO. The patterns were also independently imaged using AFM (Digital Instruments Nanoscope IIIa) operating in contact mode with SiN<sub>x</sub> cantilevers of a nominal force constant of 0.05 N/m. Scanning electron microscopy (SEM) images were taken with a Hitachi S4500 equipped with a cold field-emission electron gun.

## RESULTS AND DISCUSSION

The preliminary structural characterization of the ZnO patterns was carried out using AFM and SEM. Figures 1(a) and 1(b) show the AFM topographic images of ZnO patterns taken before and after annealing the patterns at 550 °C for 1 h in air. The lines appear uniform and remain continuous after annealing. A comparison of AFM cross-sectional scans taken before and after annealing showed that the width of the ZnO lines decreases on an average by 10% to about 300 nm and height reduces nearly by 50% to about 80 nm. We be-

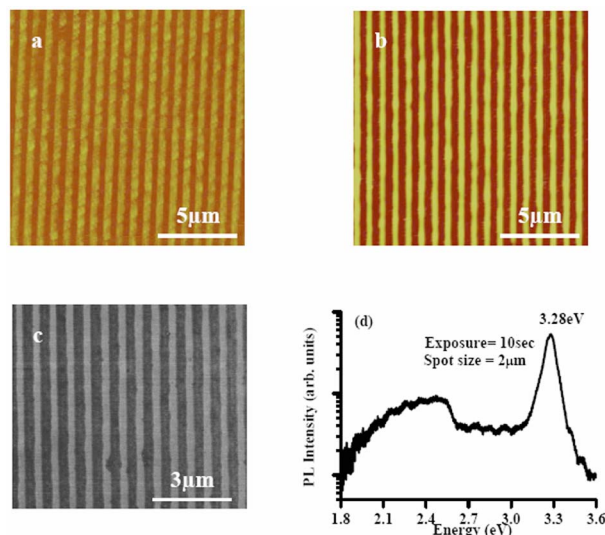


FIG. 1. (Color online) AFM topographic images (a) before and (b) after annealing at 550 °C for 1 h in air. (c) SEM image of pattern after annealing. These images were not taken at the same location. (d) Room-temperature  $\mu$ -PL spectrum of ZnO patterns showing band-edge emission at 3.28 eV and donor-acceptor pair emission below 2.5 eV.

lieve that most of this shrinkage is accommodated by patterns through generation of porous network when organics in solution are burned away during annealing step. The large shrinkage observed in height compared to width is due to relatively strong silicon–oxygen–metal bonding which is observed when solutions hydrolyze on oxide substrates.<sup>20</sup> This results in a larger constraint to reduction in width of the line compared to the height that is virtually unconstrained. The SEM image of the pattern shown in Fig. 1(c) confirms the AFM results about pattern uniformity and line continuity. The widths of these ZnO lines measured from SEM images (280 nm) are consistent with the AFM analysis. Furthermore, energy dispersive x-ray analysis (not shown here) confirms the expected Zn, O, and Si (substrate) signals from these patterns.

In order to ensure that fabricated ZnO nanopatterns are functional in terms of their photoluminescence activity, microphotoluminescence ( $\mu$ -PL) measurements were carried out using a Renishaw 2000 micro-PL setup. The room-temperature  $\mu$ -PL spectrum recorded from these patterns with 325-nm excitation is shown in Fig. 1(d). The room-temperature PL spectrum shows the characteristic near-band-edge emission at 3.28 eV and the defect-induced donor-acceptor pair emission bands below 2.5 eV. These results indicate that annealing scheme used in this work is sufficient to produce photoluminescent ZnO nanopatterns. The 2- $\mu$ m spot size used for measuring  $\mu$ -PL spectrum is still relatively a macroscopic probing because the sampling area is at least six times larger than the minimum feature size. However, it is desirable to have a characterization tool with spatial resolution better than the minimum feature size in the structure of investigation to probe the uniformity of PL emission within each line. NSOM is ideally suited for this task because it has the spatial resolution necessary to resolve the MIMIC nanopatterns of ZnO.

Figure 2 shows a set of topographic and reflection

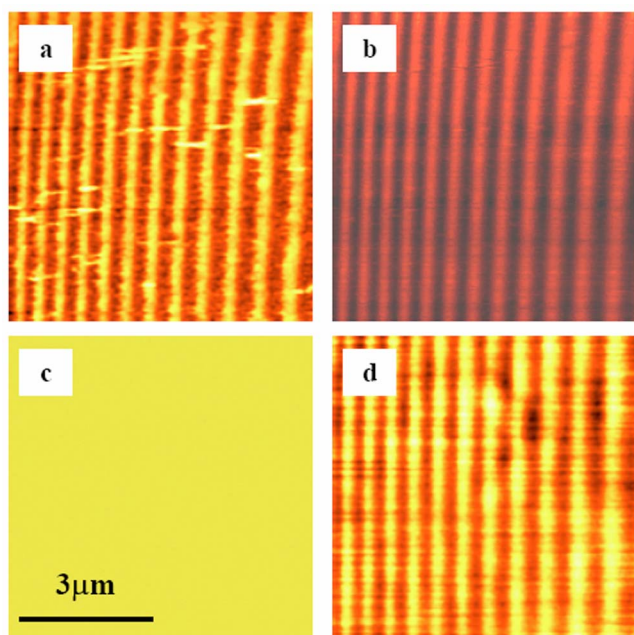


FIG. 2. (Color online) (a) Topography and (b) NSOM-optical images taken in “constant-amplitude” mode, (c) Topography, and (d) NSOM-optical images taken in “constant-height” mode. The same scale bar applies to all the images.

NSOM-optical images of ZnO patterns obtained in constant-amplitude mode and in constant-height mode. All of these images were obtained from the same specimen location by collecting reflection optical signal in far field. Figures 2(a) and 2(b) show the topographic and NSOM-optical images obtained in constant-amplitude mode. In constant-amplitude mode, the cantilevered optical fiber probe scans the sample while maintaining constant amplitude with respect to the sample using normal force feedback loop similar to the feedback control used in scanning probe microscopy. Thus, the cantilever closely tracks the surface and generates a topographic image similar to AFM. The average width of the ZnO line measured in topographic image in Fig. 2(a) (370 nm) is slightly larger than that measured using AFM [Fig. 1(a)], mainly because of the coarse tip (200 nm) used in NSOM experiments compared to the typical radius of pyramidal  $\text{SiN}_x$  tips (usually  $<50$  nm) used for contact mode AFM scans. In agreement with AFM measurements, these images show that the lines are continuous and the optical signal is uniform along each line without any dark spots. Similar to the topographic image collected with AFM [e.g., Fig. 1(b)], topographic image collected with NSOM probe [Fig. 2(a)] also shows certain topographical features, possibly individual grains within each line. However, the NSOM-optical image could not clearly resolve the exact dimensions because the aperture diameter is larger than the size of these individual features.

The NSOM-optical images taken in constant-amplitude mode are known to contain  $z$ -motion artifacts in the form of crosstalk between topographic and optical images.<sup>21,22</sup> This is evident as a strong phase-shift correlation between features in topographic and NSOM-optical images in Figs. 2(a) and 2(b). Therefore, we also measured the optical images at the

same location in constant-height mode. In constant-height mode, the cantilever is rastered on the sample without engaging it in the feedback control. In this mode, the cantilever is maintained at a constant height from the sample while scanning and thus, it does not trace any topographic feature on the surface. The optical images obtained in this mode are therefore free of  $z$ -motion artifacts. Figures 2(c) and 2(d) are topographic and NSOM-optical images, respectively, obtained in constant-height mode. As expected, topographic image is flat because the cantilever is not in feedback control. On the other hand, optical image clearly outlines ZnO nanopatterns, though with a slightly larger linewidth than seen in Fig. 2(b). In addition, some nonuniformity in the linewidths across the image is also evident in Fig. 2(d) due to limited optical resolution in  $z$  axis. This is an artifact because substrates are often not horizontally flat relative to the cantilever. Thus, while cantilever is scanning the sample at a constant height, one part of the sample will be farther from probe than another part of the sample, giving rise to observed differences in linewidths. The reduced resolution in Fig. 2(d) compared to Fig. 2(b) is due to larger tip-sample separation. It has been reported earlier by Hecht *et al.*<sup>15</sup> that spatial resolution in optical images decreases as the tip height above the sample surface increases by few nanometers. The optical image in Fig. 2(d) therefore unambiguously shows that the optical signal used to form this image is truly originating from the ZnO lines as the crosstalk with topography signal is eliminated. However, the source of contrast in this reflected optical image is not yet clear. There are two possible sources of contrast in scanned NSOM-optical images: (a) A difference in refractive index between ZnO lines and  $\text{SiO}_x$  substrate. In this case, the contrast would be simply due to the difference in reflected intensity of excited 514.5-nm light from the ZnO lines and of oxide substrate between ZnO lines. (b) Due to true localized photoluminescence from the ZnO lines. One way to identify the actual source of contrast among these two choices is to use an appropriate optical filter to cutoff the excitation laser light (i.e., 514.5 nm) because reflected light is predominantly at this wavelength. Therefore, we obtained subsequent NSOM images by selecting appropriate filter range in the monochromator before the signal reached the detector. In addition, these images were obtained in collection mode for efficient signal collection. In the collection mode operation, the excitation laser light was delivered to the sample via optical fiber whose axis is parallel to the sample normal. The optical signal from the sample is then collected with cantilevered probe of a 300-nm aperture diameter and fed via long pass filter to the monochromator with attached avalanche photodiode.

The optical and topographic images of patterns, while operating in constant-height mode in collection mode configuration, are shown in Fig. 3. As expected, this figure shows no pattern features in topographic image whereas patterns are clearly visible in the NSOM-optical image. As indicated earlier, this optical image is formed after filtering the 514.5-nm excitation laser light with a long pass filter. This image clearly shows the spatially resolved PL intensity distribution within ZnO patterns. We also noticed that maximum photon count in Fig. 3(b) decreased compared to the

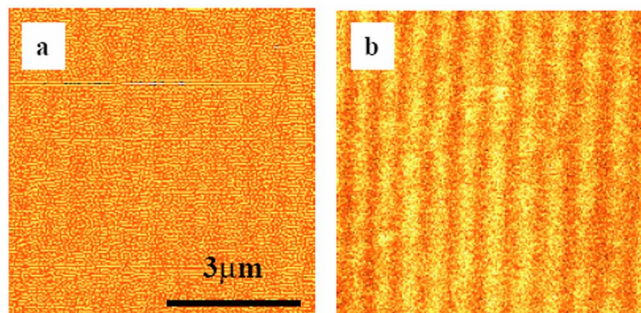


FIG. 3. (Color online) (a) Topographic and (b) NSOM-optical images of ZnO patterns obtained in collection mode configuration while operating in constant-height mode. The same scale bar applies to both images.

images in Figs. 2(b) and 2(d). The weaker scattered light intensity results in grainier NSOM-PL image. Because a long pass filter is used to form the image shown in Fig. 3(b), the contrast in this image cannot be due to difference in simple reflected light intensity from the ZnO lines and oxide surface. To further confirm this, we collected spectrum from three different locations on the sample, with and without long pass filter, by positioning the cantilever probe at various locations (Fig. 4). Figure 4(a) shows the NSOM-PL intensity image scanned while using the long pass filter prior to collecting the spectra in Fig. 4. The spectrum in Fig. 4(b) is collected from substrate, but outside the nanopatterns, without using long pass filter. Figure 4(b) spectrum shows a single narrow peak at 514.5 nm due to simple reflection from the substrate. As expected for indirect band-gap semiconductor, such as Si, no additional emission bands are visible in this spectrum. The spectra in Figs. 4(c) and 4(d) were collected from two different locations on the adjacent the ZnO lines while spectrum in Fig. 4(e) is collected between these two lines. The arrows on NSOM-optical image in Fig. 4(a) schematically indicate these locations. As the probe aperture diameter is comparable to spacing between lines, some intensity from the ZnO lines is also collected in spectrum in Fig. 4(e). However, the peak PL intensity in this region [Fig.

4(e)] is much lower when compared to those spectra recorded directly from the ZnO lines. Comparison of spectra in Figs. 4(b) and 4(c) [or 4(d)] shows that high pass filter decreases the 514.5-nm laser intensity reaching the spectrometer by almost 80%. However, the most interesting results are evident in spectra shown in Figs. 4(c) and 4(d). These spectra show characteristic broad green-yellow emission bands between 520 and 640 nm in addition to the red emission band above 650 nm. These bands are commonly observed in ZnO prepared by different chemical routes and arise due to donor-acceptor pairs (DAPs) recombination associated with defect-impurity complexes. It can now be unambiguously concluded from the spectra in Fig. 4 that the signal used to form optical images in these NSOM-optical scans is clearly the PL signal from the 300-nm ZnO nanopatterns.

We find that the ZnO PL spectra collected from nanopatterns exhibit red emission band unlike most of the reports in recent literature where PL investigation of ZnO films and ZnO nanostructures reveals only green-yellow emission bands between 510 and 640 nm.<sup>23–28</sup> A multiple peak fitting analysis of the spectrum of Figs. 4(c)–4(e) depicts that the deep gap PL from these ZnO patterns consists of at least three emission bands at approximately 560, 620, and 667 nm (corresponding to 2.2, 2.0, and 1.9 eV, respectively). The highest PL intensity in the near field is evident at 620 nm. The green-yellow emission bands are usually assigned to one of the donor and acceptor mid-band-gap defect states such as oxygen vacancies ( $V_O$ ), zinc interstitials ( $Zn_i$ ), zinc vacancies ( $V_{Zn}$ ), or antisite defects ( $O_{Zn}$ ).<sup>29</sup> Though most of the recent literature contains only report on green-yellow emission bands in ZnO, there are few earlier reports on red emission band and even a near-IR emission band at 730 nm (1.7 eV) in ZnO pellets.<sup>30–32</sup> As in the case of green-yellow emission band, the origin of red and near-IR emission bands remains an open question. Thus, the source of 667-nm PL band detected from these ZnO nanopatterns is unclear at this time. A concerted look at the vast literature on optical properties of ZnO shows that in addition to the fabrication routes,

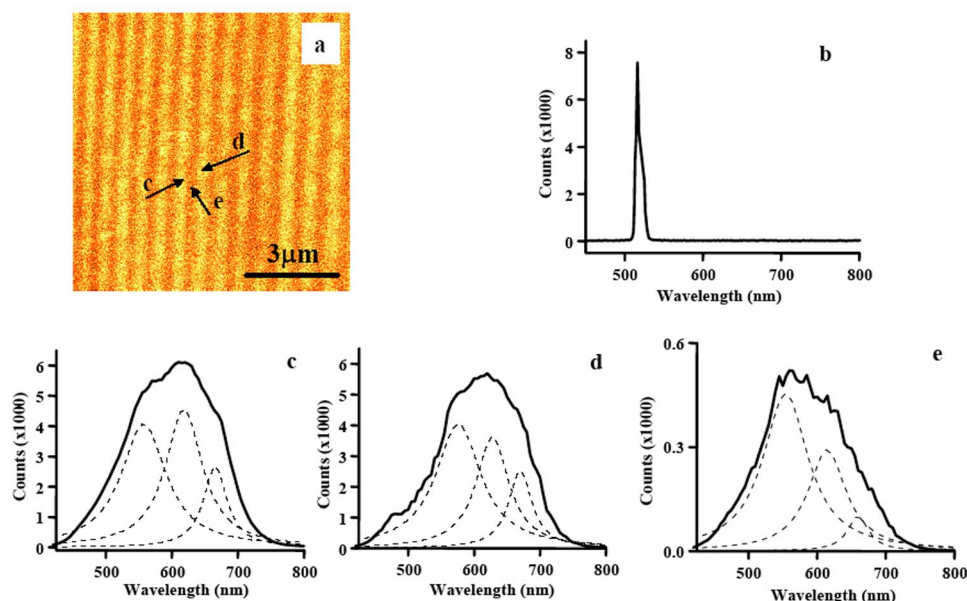


FIG. 4. (Color online) (a) NSOM-optical image of ZnO pattern. (b) Spectrum collected outside the patterns without long pass filter showing excitation laser at 514.5 nm. (c) and (d) Spectra collected from two locations on adjacent ZnO lines. (e) Spectrum collected between these two ZnO lines. Spectra shown in (c)–(e) are collected while using the long pass filter to transmit the resonantly excited photoluminescence from defect-induced bands. The dotted lines are the Lorentzian curve fits to multiple PL bands.

annealing conditions can significantly affect the PL characteristics. This is not surprising because fabrication route and processing conditions do strongly influence the concentration of various defects in material. These defects are the source of complex PL in ZnO. Thus, it remains a challenge to tailor the PL emission bands in ZnO spanning the whole visible spectrum through appropriate fabrication routes and processing parameters for potential optoelectronic applications such as polychromatic and white light displays.

In summary, we have successfully fabricated and characterized PL properties of 300-nm-wide ZnO nanopatterns. The NSOM-PL intensity images represent maps of the defect-induced photoluminescence signal originating from ZnO nanopatterns. These patterns showed significant green-yellow-red emission bands when excited with 514.5-nm laser light, at room temperature. Furthermore, this work demonstrates the capability of micromolding in capillaries as a patterning technique to fabricate 300-nm-wide functional ZnO lines with high spatial density that are continuous on oxide substrates even after annealing at 550 °C for 1 h in air. We believe that these results would be useful to understand structure-optical property relationship of nanopatterned wide-band-gap semiconductors.

## ACKNOWLEDGMENTS

We acknowledge the Nanoscale Science and Engineering Initiative of the National Science Foundation (under NSF Award Number EEC-0118025), and the U.S. Department of Energy (DOE-BES) for support of this research. This work made use of facilities at Nanoscale Integrated Fabrication, Testing and Instrumentation Center.

<sup>1</sup>T. K. Gupta, *J. Am. Ceram. Soc.* **73**, 1817 (1990).

<sup>2</sup>W. C. Shih and M. S. Wu, *J. Cryst. Growth* **137**, 319 (1994).

<sup>3</sup>D. M. Bagnall, Y. F. Chen, Z. Zhu, T. Yao, S. Koyama, M. Y. Shen, and T. Goto, *Appl. Phys. Lett.* **70**, 2230 (1997).

<sup>4</sup>Z. K. Tang, G. K. L. Wong, P. Yu, M. Kawasaki, A. Ohtomo, H. Koinuma,

and Y. Segawa, *Appl. Phys. Lett.* **72**, 3270 (1998).

<sup>5</sup>D. C. Look, *Mater. Sci. Eng., B* **80**, 383 (2001).

<sup>6</sup>M. H. Huang, Y. Y. Wu, H. Feick, N. Tran, E. Weber, and P. D. Yang, *Adv. Mater. (Weinheim, Ger.)* **13**, 113 (2001).

<sup>7</sup>Y. Dai, Y. Zhang, Q. K. Li, and C. W. Nan, *Chem. Phys. Lett.* **358**, 83 (2002).

<sup>8</sup>J. Q. Hu and Y. Bando, *Appl. Phys. Lett.* **82**, 1401 (2003).

<sup>9</sup>I. Shalish, H. Temkin, and V. Narayanamurti, *Phys. Rev. B* **69**, 245401 (2004).

<sup>10</sup>E. Kim, Y. N. Xia, and G. M. Whitesides, *J. Am. Chem. Soc.* **118**, 5722 (1996).

<sup>11</sup>N. L. Jeon, I. S. Choi, B. Xu, and G. M. Whitesides, *Adv. Mater. (Weinheim, Ger.)* **11**, 946 (1999).

<sup>12</sup>S. Seraji, Y. Wu, N. E. Jewell-Larson, M. J. Forbess, S. J. Limmer, T. P. Chou, and G. Z. Cao, *Adv. Mater. (Weinheim, Ger.)* **12**, 1421 (2000).

<sup>13</sup>M. Heule, J. Schell, and L. J. Gauckler, *J. Am. Ceram. Soc.* **86**, 407 (2003).

<sup>14</sup>U. Ben-Ami *et al.*, *Appl. Phys. Lett.* **73**, 1619 (1998).

<sup>15</sup>B. Hecht, B. Sick, U. P. Wild, V. Deckert, R. Zenobi, O. J. F. Martin, and D. W. Pohl, *J. Chem. Phys.* **112**, 7761 (2000).

<sup>16</sup>E. Betzig and J. K. Trautman, *Science* **257**, 189 (1992).

<sup>17</sup>M. J. Fasaloka, L. S. Goldner, J. Hwang, A. M. Urbas, P. DeRege, T. Swager, and E. L. Thomas, *Phys. Rev. Lett.* **90**, 016107 (2003).

<sup>18</sup>J. C. Johnson, H. Q. Yan, R. D. Schaller, P. B. Petersen, P. D. Yang, and R. J. Saykally, *Nano Lett.* **2**, 279 (2002).

<sup>19</sup>O. Tikhomirov, H. Jiang, and J. Levy, *Appl. Phys. Lett.* **77**, 2048 (2000).

<sup>20</sup>I. Ichinose, H. Senzu, and T. Kunitake, *Chem. Mater.* **9**, 1296 (1997).

<sup>21</sup>B. Hecht, H. Bielefeldt, Y. Inoüye, D. W. Pohl, and L. Novotny, *J. Appl. Phys.* **81**, 2492 (1997).

<sup>22</sup>R. Carminati, A. Madrazo, M. NietoVesperinas, and J. J. Greffet, *J. Appl. Phys.* **82**, 501 (1997).

<sup>23</sup>K. Park, J. S. Lee, M. Y. Sung, and S. Kim, *Jpn. J. Appl. Phys., Part 1* **41**, 7317 (2002).

<sup>24</sup>X. Liu, Ph.D. thesis, Northwestern University, Evanston, 2003.

<sup>25</sup>S. Choopun, R. D. Vispute, W. Noch, A. Balsamo, R. P. Sharma, T. Venkatesan, A. Iliadis, and D. C. Look, *Appl. Phys. Lett.* **75**, 3947 (1999).

<sup>26</sup>T. Aoki, Y. Hatanaka, and D. C. Look, *Appl. Phys. Lett.* **76**, 3257 (2000).

<sup>27</sup>S. B. Zhang, S. H. Wei, and A. Zunger, *Phys. Rev. B* **63**, 075407 (2001).

<sup>28</sup>K. Vanheusden, C. H. Seager, W. L. Warren, D. R. Tallant, and J. A. Voigt, *Appl. Phys. Lett.* **68**, 403 (1996).

<sup>29</sup>B. X. Lin, Z. X. Fu, and Y. B. Jia, *Appl. Phys. Lett.* **79**, 943 (2001).

<sup>30</sup>Y. M. Gerbshtein and Y. M. Zelikin, *Opt. Spectrosc.* **28**, 521 (1970).

<sup>31</sup>W. Lehmann, *J. Electrochem. Soc.* **115**, 538 (1968).

<sup>32</sup>R. B. Lauer, *J. Phys. Chem. Solids* **34**, 249 (1973).